Enhanced Jamming Suppression in Colocated MIMO Radar with Fluid Antenna Array

Linlong Wu[†], Bhavani Shankar M. R.[†], Wei Liu[‡] and Björn Ottersten[†]
[†]*Interdisciplinary Center for Security, Reliability and Trust (SnT), University of Luxembourg*
[‡]*School of Electronic Engineering and Computer Science, Queen Mary University of London*
Email:{linlong.wu; bhavani.shankar; bjorn.ottersten}@uni.lu; w.liu@qmul.ac.uk

***Abstract*—Beyond traditional solid-state antenna, fluid antennas (FAs) exhibit unparalleled reconfigurability, drawing significant interest for applications in wireless communications and radar. This paper presents a design of FA array (FAA) MIMO radar for improved target detection in the presence of jammers, highlighting the advantages of FAA in sensing scenarios. By utilizing flexible positioning of FAAs, we introduce the antenna position vector (APV) as a design variable, in addition to waveforms, aiming to maximize the signal-to-interference plus noise ratio (SINR) with constraints to maintain waveform unimodularity and avoid FA coupling. The formulated nonconvex problem is tackled by an iterative algorithm based on the block majorization-minimization framework. Each iteration involves solving linearly constrained quadratic programming problems for APV optimization and updating the waveforms via a closed-form solution. Simulation results reveal that the designed APVs of the transmit and receiving FAAs can automatically balance angular resolution and ambiguity, which together with the optimized waveform, significantly enhances the SINR through enhanced jamming suppression. This improvement is attributed to increased flexibility across spatial and frequency dimensions facilitated by the FAAs.**

***Index Terms*—MIMO radar, Fluid antenna array, waveform design, jamming suppression, SINR maximization**

I. Introduction

Using multiple transmit and receive antennas with independent radio-frequency (RF) chains, MIMO radar can achieve enhanced spatial resolution and more effective target detection [1]. Notably, a forward push to the advancement of MIMO radar is provided by the waveform design [2]. The independence of multiple RF chains facilitates the transmission of diverse waveforms, and advancements in hardware and computational resources enable real-time implementation of complex waveforms. Consequently, there is a burgeoning literature on signal processing methods and algorithms to explore various facets of waveform design. To name a few, integrated sidelobe level (ISL) based waveform designs have been studied over the last decades to ensure the orthogonality among waveforms [3–5]. To improve the detection performance, the signal-to-noise ratio (SNR) or signal-to-interference plus noise ratio (SINR) is maximized by designing the waveform adaptively [6–8]. To facilitate efficient spectral management, waveform design schemes under the spectrally crowded environment or co-existence with communications [9–11] have also been extensively studied. From the perspective of information theory, mutual information (MI) is explored for radar waveform design for extended targets [12, 13]. The scope of innovation is further expanded by considering emerging technologies such as reconfigurable intelligent surface [14].

In addition to waveform design, array design has also been studied. Recently, fluid antennas (FAs) have garnered significant research interest. In a broader sense, beyond its initial liquid-state concept, fluid antenna refers to any controllable fluidic conductive structure, movable mechanical antenna structure, or even reconfigurable RF pixels that are capable of adjusting their shape and position to modify gain, radiation patterns, frequencies, and other characteristics [15–18]. As a natural extension, fluid antenna array (FAA) is increasingly recognized for its potential in next-generation wireless communications and sensing. The work in [19] demonstrated that a single-antenna FA system, even in a constrained space, can outperform a multi-antenna system using Maximum Ratio Combining (MRC) in Rayleigh fading channels. The multiplexing gain through FA adaptable positioning was highlighted in [20] for fluid antenna multiple access (FAMA). Further, the investigation in [21] focused on enhancing physical-layer security using Movable Antenna (MA) arrays by optimizing both beamforming and MA positioning. Additionally, incorporating FAAs into over-the-air computation systems was shown to enhance wireless data aggregation by reducing the mean square error (MSE) of the estimates in [22].

In the context of MIMO radar, the features of FAA, combined with the diversity of transmit waveforms, are anticipated to further expand MIMO radar capabilities. Specifically, each fluid antenna's ability to reshape and relocate alters its radiation position on the array plane, effectively simulating continuous antenna movement. This introduces a new Degree of Freedom (DoF), extending independence from RF chains to the antennas themselves, allowing fully independent signal emission in not only characteristics but also spatial positioning. Therefore, in this work, the FAA-MIMO radar is investigated for enhanced target detection in the presence of multiple jamming signals, where the SINR is maximized by optimizing waveforms and FAAs, considering the requirement of mutual coupling and amplifier efficiency as constraints. To address challenges of the formulated nonconvex SINR maximization problem, an iterative algorithm is developed based on the block majorization-minimization (MM) method [23, 24], where the problems to be solved at each iteration become convex and quadratic. The proposed algorithm ensures that the FAAs can be fine-tuned to balance angular resolution against ambiguity effectively. Through simulations, it is revealed that the synergistic optimization of FAA and waveform significantly enhances SINR performance, surpassing the improvement achieved by waveform optimization alone. This advancement is attributed to the enhanced flexibility of FAA-MIMO in both spatial and frequency dimensions.

The rest of this paper is organized as follows. Section II develops the signal model for the FAA-MIMO radar and then formulates the problem. The proposed solution is developed in Section III. Simulation results are presented in Section VI and conclusions are drawn in Section V.

Notations: Boldface lowercase and uppercase letters denote the vectors and matrices, respectively. The notations $(\cdot)^T$, $(\cdot)^*$ and $(\cdot)^H$ denote transpose, conjugate, and Hermitian transpose, respectively; $\mathbf{I}_L$ denotes the $L \times L$ identity matrix; $\otimes$ denotes the Kronecker

The work of L. Wu, B. Shankar and B. Ottersten was supported by the FNR CORE INTER project under grant C20/IS/14799710/SENCOM. The work of W. Liu was supported by the UK EPSRC under grant EP/V009419/2.

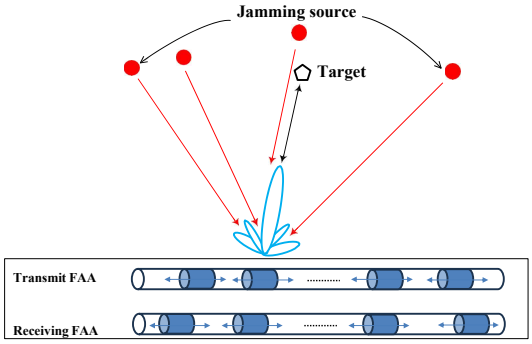

Figure 1. FAA-MIMO radar for target detection with jamming signals.

product; $\arg(\cdot)$ denotes the phase value; $\Re\{\cdot\}$ and $\Im\{\cdot\}$ are the real and imaginary parts, respectively.

II. Signal Model and Problem Formulation

The considered scenario is shown in Fig. 1, where the co-located FAA-equipped MIMO radar is deployed to detect a single target with the existence of multiple jamming signals at different angular directions. The transmit and receiving FAAs have N_t and N_r FAs, respectively. The waveform emitted by the n-th transmit FA is denoted by $\mathbf{s}_n \in \mathbb{C}^L$ with L being the waveform length, and further the waveform matrix is defined as $\mathbf{S} = [\mathbf{s}_1, \mathbf{s}_2, \ldots, \mathbf{s}_{N_t}] \in \mathbb{C}^{L\times N_t}$. The antenna position vector (APV) of the transmit FAA is defined as $\dot{\mathbf{x}} = [\dot{x}_1, \dot{x}_2, ..., \dot{x}_{N_t}] \in \mathbb{C}^{N_t}$, where $\dot{x}_n \in [0, R]$ denotes the position of the n-th transmit FA on a line segment of length R. Similarly, the APV $\ddot{\mathbf{x}} = [\ddot{x}_1, \ddot{x}_2, ..., \ddot{x}_{N_r}] \in \mathbb{C}^{N_r}$ with $\ddot{x}_n \in [0, R]$ is defined for the receiving FAA. Note that all FAs can move freely within the line segments because of the fluid nature.

Assuming the target is in direction θ_T, the received signal is

$$\mathbf{y} = \alpha_T \left[\left(\mathbf{a}_r\left(\theta_T, \ddot{\mathbf{x}}\right) \mathbf{a}_t^T\left(\theta_T, \dot{\mathbf{x}}\right) \right) \otimes \mathbf{I}_L \right] \mathbf{s} + \mathbf{n}, \tag{1}$$

where α_T accounts for the target complex reflection with $\mathbb{E}\left[|\alpha_T|^2\right] = \sigma_T$, $\mathbf{s} = \mathrm{vec}\left(\mathbf{S}\right)$, $\mathbf{a}_t\left(\theta_T, \dot{\mathbf{x}}\right)$ and $\mathbf{a}_r\left(\theta_T, \ddot{\mathbf{x}}\right)$ are the transmit and receiving steering vectors respectively given by

$$\begin{cases} \mathbf{a}_t\left(\theta, \dot{\mathbf{x}}\right) = \left[e^{-j\frac{2\pi}{\lambda}\sin\theta\dot{x}_1}, e^{-j\frac{2\pi}{\lambda}\sin\theta\dot{x}_2}, ..., e^{-j\frac{2\pi}{\lambda}\sin\theta\dot{x}_{N_t}} \right]^T \\ \mathbf{a}_r\left(\theta, \ddot{\mathbf{x}}\right) = \left[e^{-j\frac{2\pi}{\lambda}\sin\theta\ddot{x}_1}, e^{-j\frac{2\pi}{\lambda}\sin\theta\ddot{x}_2}, ..., e^{-j\frac{2\pi}{\lambda}\sin\theta\ddot{x}_{N_r}} \right]^T, \end{cases} \tag{2}$$

and $\mathbf{n}$ is the signal-independent interference.

For the interference $\mathbf{n}$, it consists of white noise and several jamming signals modeled as

$$\mathbf{n} = \mathbf{n}_0 + \sum_{p=1}^{P} \left[\mathbf{a}_r\left(\theta_p, \ddot{\mathbf{x}}\right) \otimes \mathbf{I}_L \right] \mathbf{c}_p, \tag{3}$$

where $\mathbf{n}_0 \sim \mathcal{CN}\left(\mathbf{0}, \sigma_0 \mathbf{I}_{N_r L}\right)$ is the ambient noise, P is the number of jamming signals, $\mathbf{c}_p$ is the p-th jamming signal transmitted from the angular direction θ_p occupying the frequency band $[f_1^p, f_2^p]$ and is independent of the transmit waveforms $\mathbf{s}$. We further model the jamming signal by $\mathbf{c}_p \sim \mathcal{CN}\left(\mathbf{0}, \mathbf{R}_p\right)$ with $\mathbf{R}_p \in \mathbb{C}^{L\times L}$ being its covariance matrix [25]. Assuming $\mathbf{n}_0$ and the jamming signals are independent of each other, the covariance matrix of $\mathbf{n}$ is

$$\mathbf{R}\left(\ddot{\mathbf{x}}\right) = \sigma_0 \mathbf{I}_{N_r L} + \sum_{p=1}^{P} \left[\mathbf{a}_r\left(\theta_p, \ddot{\mathbf{x}}\right) \otimes \mathbf{I}_L \right] \mathbf{R}_p \left[\mathbf{a}_r\left(\theta_p, \ddot{\mathbf{x}}\right) \otimes \mathbf{I}_L \right]^H. \tag{4}$$

For the transmit and receiving FAAs, the constraints of the APVs $\dot{\mathbf{x}}$ and $\ddot{\mathbf{x}}$ are

$$\begin{cases} 0 \le \dot{x}_n, \ddot{x}_n \le R, & (a) \\ \dot{x}_n - \dot{x}_{n-1} \ge r_0, \ddot{x}_n - \ddot{x}_{n-1} \ge r_0, & (b) \end{cases} \tag{5}$$

where (a) is due to the physical limitation of the positioning interval $[0, R]$, and(b) restricts the minimal spacing between the two adjacent FAs to avoid severe mutual coupling.

At the receiver, the SINR after mismatch filtering is

$$\mathrm{SINR}(\mathbf{s}, \dot{\mathbf{x}}, \ddot{\mathbf{x}}) = \sigma_T \mathbf{s}^H \mathbf{H}^H\left(\dot{\mathbf{x}}, \ddot{\mathbf{x}}\right) \mathbf{R}\left(\ddot{\mathbf{x}}\right)^{-1} \mathbf{H}\left(\dot{\mathbf{x}}, \ddot{\mathbf{x}}\right) \mathbf{s},$$

where $\mathbf{H}\left(\dot{\mathbf{x}}, \ddot{\mathbf{x}}\right) = \left(\mathbf{a}_r\left(\theta_T, \ddot{\mathbf{x}}\right) \mathbf{a}_t^T\left(\theta_T, \dot{\mathbf{x}}\right)\right) \otimes \mathbf{I}_L$. Therefore, the problem formulated as

$$\mathcal{P} \begin{cases} \underset{\mathbf{s}, \dot{\mathbf{x}}, \ddot{\mathbf{x}}}{\text{maximize}} & \mathbf{s}^H \mathbf{H}^H\left(\dot{\mathbf{x}}, \ddot{\mathbf{x}}\right) \mathbf{R}\left(\ddot{\mathbf{x}}\right)^{-1} \mathbf{H}\left(\dot{\mathbf{x}}, \ddot{\mathbf{x}}\right) \mathbf{s} \\ \text{subject to} & \mathbf{s} \in \mathcal{S}, \dot{\mathbf{x}}, \ddot{\mathbf{x}} \in \mathcal{X} \end{cases} \tag{6}$$

where $\mathcal{S} = \{\mathbf{s} | |s_\ell| = 1\}$ requires the constant-modulus waveform to ensure the power efficiency of hardware such as amplifiers, and $\mathcal{X} = \{\mathbf{x} | 0 \le x_n \le R, x_n - x_{n-1} \ge r_0, \forall n\}$. Solving problem (6) via joint waveform-FAA design yields a desired angle-frequency profile.

III. Joint Waveform Design and FA Positioning

First of all, we have

$$\mathbf{H}\left(\dot{\mathbf{x}}, \ddot{\mathbf{x}}\right)\mathbf{s} = \mathbf{\Psi}\left(\mathbf{s}, \ddot{\mathbf{x}}\right)\mathbf{a}_t\left(\theta_T, \dot{\mathbf{x}}\right) = \mathbf{\Phi}\left(\mathbf{s}, \dot{\mathbf{x}}\right)\mathbf{a}_r\left(\theta_T, \ddot{\mathbf{x}}\right), \tag{7}$$

where $\mathbf{\Psi}\left(\mathbf{s}, \ddot{\mathbf{x}}\right) = \mathbf{a}_r\left(\theta_T, \ddot{\mathbf{x}}\right) \otimes \mathbf{S}$ and $\mathbf{\Phi}\left(\mathbf{s}, \dot{\mathbf{x}}\right) = \mathbf{I}_{N_r L} \otimes \left(\mathbf{S}\mathbf{a}_t\left(\theta_T, \dot{\mathbf{x}}\right)\right)$. By applying the framework of block MM, we solve three subproblems of the variables $\mathbf{s}$, $\dot{\mathbf{x}}$ and $\ddot{\mathbf{x}}$ at each iteration:

$$\mathcal{P}_{\mathbf{s}}: \underset{\mathbf{s}\in\mathcal{S}}{\text{maximize}} \quad \mathbf{s}^H \mathbf{H}^H \mathbf{R}^{-1} \mathbf{H} \mathbf{s} \tag{8}$$

$$\mathcal{P}_{\dot{\mathbf{x}}}: \underset{\dot{\mathbf{x}}\in\mathcal{X}}{\text{maximize}} \quad \mathbf{a}_t^H\left(\theta_T, \dot{\mathbf{x}}\right) \mathbf{\Psi}^H \mathbf{R}^{-1} \mathbf{\Psi} \mathbf{a}_t\left(\theta_T, \dot{\mathbf{x}}\right) \tag{9}$$

$$\mathcal{P}_{\ddot{\mathbf{x}}}: \underset{\ddot{\mathbf{x}}\in\mathcal{X}}{\text{maximize}} \quad \mathbf{a}_{\mathrm{r}}^H\left(\theta_T, \ddot{\mathbf{x}}\right) \mathbf{\Phi}^H \mathbf{R}\left(\ddot{\mathbf{x}}\right)^{-1} \mathbf{\Phi} \mathbf{a}_r\left(\theta_T, \ddot{\mathbf{x}}\right) \tag{10}$$

Note that problem $\mathcal{P}_{\mathbf{s}}$ is well-studied and can be solved iteratively by methods such as power-like iteration [26]. We focus on solving $\mathcal{P}_{\dot{\mathbf{x}}}$ and $\mathcal{P}_{\ddot{\mathbf{x}}}$ in the following subsections.

A. Solving Problem $\mathcal{P}_{\dot{\mathbf{x}}}$ for Transmit FAA

By defining $\mathbf{M} = \mathbf{\Psi}^H \mathbf{R}^{-1} \mathbf{\Psi} \in \mathbb{C}^{N_t \times N_t}$, the objective function of $\mathcal{P}_{\dot{\mathbf{x}}}$ is expressed as

$$\mathbf{a}_t^H\left(\theta_T, \dot{\mathbf{x}}\right) \mathbf{M} \mathbf{a}_t\left(\theta_T, \dot{\mathbf{x}}\right) = \sum_{n=1}^{N_t} M_{n,n} + \sum_{i=j+1}^{N_t} \sum_{j=1}^{N_t} 2\left|M_{i,j}\right| \cos\left(\left(\mathbf{e}_i - \mathbf{e}_j\right)^T \dot{\mathbf{x}} \frac{2\pi}{\lambda} \sin\theta_T + \arg\left\{M_{i,j}\right\} \right)$$

where $\mathbf{e}_i \in \mathbb{C}^{N_t}$ is the selection vector with the i-th element being 1 and the rest being 0. Noting that $M_{n,n}$ is independent of $\dot{\mathbf{x}}$, problem $\mathcal{P}_{\dot{\mathbf{x}}}$ can be rewritten equivalently as

$$\widetilde{\mathcal{P}}_{\dot{\mathbf{x}}} \begin{cases} \underset{\dot{\mathbf{x}}}{\text{maximize}} & \sum_{i=j+1}^{N_t} \sum_{j=1}^{N_t} \left\{ 2\left|M_{i,j}\right| \cos\left(\left(\mathbf{e}_i - \mathbf{e}_j\right)^T \dot{\mathbf{x}} \frac{2\pi}{\lambda} \sin\theta_T + \arg\left\{M_{i,j}\right\} \right) \right\} \\ \text{subject to} & \dot{\mathbf{x}} \in \mathcal{X} \end{cases} \tag{11}$$

Denote the objective function of $\widetilde{\mathcal{P}}_{\dot{\mathbf{x}}}$ by $f_1(\dot{\mathbf{x}})$, the following lemma provides a surrogate function of $f_1(\dot{\mathbf{x}})$.

Lemma III.1. *A minorizor denoted by $\ell(\dot{\mathbf{x}}, \dot{\mathbf{x}}_m)$ of $f_1(\dot{\mathbf{x}})$ is*

$$\begin{aligned}\ell_1(\dot{\mathbf{x}}, \dot{\mathbf{x}}_m) = &-\sum_{i=j+1}^{N_t}\sum_{j=1}^{N_t}|M_{i,j}|\left[(\mathbf{e}_i-\mathbf{e}_j)^T(\dot{\mathbf{x}}-\dot{\mathbf{x}}_m)\frac{2\pi}{\lambda}\sin\theta_T\right]^2\\ &-\left\{\sum_{i=j+1}^{N_t}\sum_{j=1}^{N_t}\sin\left((\mathbf{e}_i-\mathbf{e}_j)^T\dot{\mathbf{x}}_m\frac{2\pi}{\lambda}\sin\theta_T+\arg\{M_{i,j}\}\right)\right.\\ &\left.(\mathbf{e}_i-\mathbf{e}_j)^T(\dot{\mathbf{x}}-\dot{\mathbf{x}}_m)\,2\,|M_{i,j}|\frac{2\pi}{\lambda}\sin\theta_T\right\}+\textit{const.}\end{aligned} \tag{12}$$

which holds that $\ell_1(\dot{\mathbf{x}}, \dot{\mathbf{x}}_m) \le f_1(\dot{\mathbf{x}})$ with equality when $\dot{\mathbf{x}} = \dot{\mathbf{x}}_m$.

Proof: It holds that $\cos(x) \ge -\frac{1}{2}(x-a)^2 - \sin(a)(x-a) + \cos(a)$. The expression of $\ell(\dot{\mathbf{x}}, \dot{\mathbf{x}}_m)$ is obtained after substituting $x = (\mathbf{e}_i-\mathbf{e}_j)^T\dot{\mathbf{x}}\frac{2\pi}{\lambda}\sin\theta_T + \arg\{M_{i,j}\}$ into this inequality. ∎

Therefore, the minorized problem of $\widetilde{\mathcal{P}}_{\dot{\mathbf{x}}}$ is

$$\begin{aligned}\underset{\dot{\mathbf{x}}\in\mathcal{X}}{\text{maximize}}\quad &\sum_{i=j+1}^{N_t}\sum_{j=1}^{N_t}\left\{\dot{w}_{i,j}\left[(\mathbf{e}_i-\mathbf{e}_j)^T(\dot{\mathbf{x}}-\dot{\mathbf{x}}_m)\right]^2\right.\\ &\left.+\dot{u}_{i,j}(\mathbf{e}_i-\mathbf{e}_j)^T(\dot{\mathbf{x}}-\dot{\mathbf{x}}_m)\right\},\end{aligned} \tag{13}$$

where $\dot{w}_{i,j} = -|M_{i,j}|\left(\frac{2\pi}{\lambda}\sin\theta_T\right)^2$ and

$$\dot{u}_{i,j} = -|M_{i,j}|\frac{4\pi}{\lambda}\sin\theta_T\sin\left((\mathbf{e}_i-\mathbf{e}_j)^T\dot{\mathbf{x}}_m\frac{2\pi}{\lambda}\sin\theta_T+\arg\{M_{i,j}\}\right).$$

This problem can be further simplified as

$$\underset{\dot{\mathbf{x}}\in\mathcal{X}}{\text{maximize}}\quad \dot{\mathbf{x}}^T\mathbf{G}\dot{\mathbf{x}} + \mathbf{h}^T\dot{\mathbf{x}}, \tag{14}$$

where $\mathbf{G} = \sum_{i=j+1}^{N_t}\sum_{j=1}^{N_t}\dot{w}_{i,j}(\mathbf{e}_i-\mathbf{e}_j)(\mathbf{e}_i-\mathbf{e}_j)^T \preceq \mathbf{0}$ and $\mathbf{h} = -2\mathbf{G}\dot{\mathbf{x}}_m + \sum_{i=j+1}^{N_t}\sum_{j=1}^{N_t}\dot{u}_{i,j}(\mathbf{e}_i-\mathbf{e}_j)$. This problem is convex and hence can be solved efficiently by existing solvers.

B. Solving Problem $\mathcal{P}_{\ddot{\mathbf{x}}}$ for Receiving FAA

Note $\ddot{\mathbf{x}}$ appears inside the matrix inverse of the objective function.

Lemma III.2. *[7] A minorizor denoted by $\ell_2(\ddot{\mathbf{x}}, \ddot{\mathbf{x}}_m)$ of the objective function denoted by $f_2(\ddot{\mathbf{x}})$ of $\mathcal{P}_{\ddot{\mathbf{x}}}$ is*

$$\begin{aligned}\ell_2(\ddot{\mathbf{x}}, \ddot{\mathbf{x}}_m) = &-\sum_{p=1}^{P}\boldsymbol{g}_m^H(\mathbf{a}_r(\theta_p,\ddot{\mathbf{x}})\otimes\mathbf{I}_L)\mathbf{R}_p(\mathbf{a}_r(\theta_p,\ddot{\mathbf{x}})\otimes\mathbf{I}_L)^H\boldsymbol{g}_m\\ &+2\Re\left\{\boldsymbol{g}_m^H\boldsymbol{\Phi}\mathbf{a}_r(\theta_T,\ddot{\mathbf{x}})\right\}-\sigma_0\|\boldsymbol{g}_m\|_2^2\end{aligned} \tag{15}$$

with

$$\begin{aligned}\mathbf{g}_m = &\left[\sigma_0\mathbf{I}_{N_rL}+\left\{\sum_{p=1}^{P}(\mathbf{a}_r(\theta_p,\ddot{\mathbf{x}}_m)\otimes\mathbf{I}_L)\mathbf{R}_p\right.\right.\\ &\left.\left.(\mathbf{a}_r(\theta_p,\ddot{\mathbf{x}}_m)\otimes\mathbf{I}_L)^H\right\}\right]^{-1}\boldsymbol{\Phi}\mathbf{a}_r(\theta_T,\ddot{\mathbf{x}}_m).\end{aligned} \tag{16}$$

It holds that $\ell_2(\ddot{\mathbf{x}}, \ddot{\mathbf{x}}_m) \le f_2(\ddot{\mathbf{x}})$ with equality when $\ddot{\mathbf{x}} = \ddot{\mathbf{x}}_m$.

Applying Lemma III.2 on $\mathcal{P}_{\ddot{\mathbf{x}}}$, the minorized problem is

$$\begin{aligned}\underset{\ddot{\mathbf{x}}\in\mathcal{X}}{\text{maximize}}\quad &-\left\{\sum_{p=1}^{P}\mathbf{g}_m^H[\mathbf{a}_r(\theta_p,\ddot{\mathbf{x}})\otimes\mathbf{I}_L]\mathbf{R}_p\right.\\ &\left.[\mathbf{a}_r(\theta_p,\ddot{\mathbf{x}})\otimes\mathbf{I}_L]^H\mathbf{g}_m\right\}+2\Re\left\{\mathbf{g}_m^H\boldsymbol{\Phi}\mathbf{a}_r(\theta_T,\ddot{\mathbf{x}}_m)\right\}.\end{aligned} \tag{17}$$

Denoting $\mathbf{g}_m = [g_{m,1},\ldots,g_{m,N_rL}]^T_*$, it holds that $[\mathbf{a}_r(\theta_p,\ddot{\mathbf{x}})\otimes\mathbf{I}_L]^H\mathbf{g}_m = \left(\widetilde{\mathbf{G}}_m\mathbf{a}_r(\theta_p,\ddot{\mathbf{x}})\right)^*$, where $\widetilde{\mathbf{g}}_{m,\ell} = \left[g_{m,\ell}, g_{m,L+\ell},\ldots,g_{m,(N_r-1)L+\ell}\right]^T$ and $\widetilde{\mathbf{G}}_m = [\widetilde{\mathbf{g}}_{m,1}\ldots,\widetilde{\mathbf{g}}_{m,L}]^H$. Furthermore, we have

$$\begin{aligned}&\mathbf{g}_m^H[\mathbf{a}_r(\theta_p,\ddot{\mathbf{x}}_m)\otimes\mathbf{I}_L]\mathbf{R}_p[\mathbf{a}_r(\theta_p,\ddot{\mathbf{x}}_m)\otimes\mathbf{I}_L]^H\mathbf{g}_m\\ =&\mathbf{a}_r^H(\theta_p,\ddot{\mathbf{x}}_m)\widetilde{\mathbf{G}}_m^H\mathbf{R}_p^*\widetilde{\mathbf{G}}_m\mathbf{a}_r(\theta_p,\ddot{\mathbf{x}}_m),\end{aligned} \tag{18}$$

With $\boldsymbol{\Xi}_p = \widetilde{\mathbf{G}}_m^H\mathbf{R}_p^*\widetilde{\mathbf{G}}_m$, the first term in the objective function of problem (17) can be rewritten as

$$\begin{aligned}&\sum_{p=1}^{P}\mathbf{a}_r^H(\theta_p,\ddot{\mathbf{x}}_m)\boldsymbol{\Xi}_p\mathbf{a}_r(\theta_p,\ddot{\mathbf{x}}_m) = \sum_{p=1}^{P}\sum_{n=1}^{N_r}\Xi_{n,n}^p+\\ &\sum_{p=1}^{P}\sum_{i=j+1}^{N_r}\sum_{j=1}^{N_r}2\left|\Xi_{i,j}^p\right|\cos\left((\mathbf{e}_i-\mathbf{e}_j)^T\ddot{\mathbf{x}}\frac{2\pi}{\lambda}\sin\theta_p+\arg\left\{\Xi_{i,j}^p\right\}\right)\end{aligned} \tag{19}$$

Similarly, the term $\Re\left\{\mathbf{v}^H\mathbf{a}_r(\theta_T,\ddot{\mathbf{x}})\right\}$ can be rewritten as

$$\Re\left\{\mathbf{v}^H\mathbf{a}_r(\theta_T,\ddot{\mathbf{x}})\right\} = \sum_{n=1}^{N_r}|v_n|\cos\left(\frac{2\pi}{\lambda}\sin\theta_T\mathbf{e}_n^T\ddot{\mathbf{x}}+\arg\{v_n\}\right),$$

where $\mathbf{v} = 2\boldsymbol{\Phi}^H\mathbf{g}_m$. Therefore, problem (17) is equivalent to

$$\widetilde{\mathcal{P}}_{\ddot{\mathbf{x}}}\begin{cases}\underset{\ddot{\mathbf{x}}\in\mathcal{X}}{\text{maximize}}\quad -\left\{\sum_{p=1}^{P}\sum_{i=j+1}^{N_r}\sum_{j=1}^{N_r}2\left|\Xi_{i,j}^p\right|\right.\\ \qquad\left.\cos\left((\mathbf{e}_i-\mathbf{e}_j)^T\ddot{\mathbf{x}}\frac{2\pi}{\lambda}\sin\theta_p+\arg\left\{\Xi_{i,j}^p\right\}\right)\right\}\\ \qquad+\sum_{n=1}^{N_r}|v_n|\cos\left(\frac{2\pi}{\lambda}\sin\theta_T\mathbf{e}_n^T\ddot{\mathbf{x}}+\arg\{v_n\}\right).\end{cases} \tag{20}$$

Lemma III.3. *The objective function of $\widetilde{\mathcal{P}}_{\ddot{\mathbf{x}}}$ denoted by $f_3(\ddot{\mathbf{x}})$ is minorized by*

$$\begin{aligned}\ell_3(\ddot{\mathbf{x}}, \ddot{\mathbf{x}}_m) = &f_3(\ddot{\mathbf{x}}_m)+\sum_{i=j+1}^{N_r}\sum_{j=1}^{N_r}\ddot{w}_{i,j}\left[(\mathbf{e}_i-\mathbf{e}_j)^T(\ddot{\mathbf{x}}-\ddot{\mathbf{x}}_m)\right]^2\\ &+\sum_{i=j+1}^{N_r}\sum_{j=1}^{N_r}\ddot{u}_{i,j}\left[(\mathbf{e}_i-\mathbf{e}_j)^T(\ddot{\mathbf{x}}-\ddot{\mathbf{x}}_m)\right]\\ &+\sum_{n=1}^{N_r}\beta_{n,1}\left[\mathbf{e}_n^T(\ddot{\mathbf{x}}-\ddot{\mathbf{x}}_m)\right]^2+\sum_{n=1}^{N_r}\beta_{n,2}\left[\mathbf{e}_n^T(\ddot{\mathbf{x}}-\ddot{\mathbf{x}}_m)\right],\end{aligned} \tag{21}$$

where $\ddot{w}_{i,j} = -\sum_{p=1}^{P}\left|\Xi_{i,j}^p\right|\left(\frac{2\pi}{\lambda}\sin\theta_p\right)^2 \le 0$,

$$\ddot{u}_{i,j} = \sum_{p=1}^{P}\left|\Xi_{i,j}^p\right|\frac{4\pi}{\lambda}\sin\theta_p\sin\left((\mathbf{e}_i-\mathbf{e}_j)^T\ddot{\mathbf{x}}_m\frac{2\pi}{\lambda}\sin\theta_p+\arg\left\{\Xi_{i,j}^p\right\}\right),$$

$\beta_{n,1} = -|v_n|\frac{1}{2}\left(\frac{2\pi}{\lambda}\sin\theta_T\right)^2 \le 0$, *and*

$$\beta_{n,2} = -|v_n|\frac{2\pi}{\lambda}\sin\theta_T\sin\left[\mathbf{e}_n^T\ddot{\mathbf{x}}_m\frac{2\pi}{\lambda}\sin\theta_T+\arg\{v_n\}\right].$$

It holds that $\ell_3(\ddot{\mathbf{x}}, \ddot{\mathbf{x}}_m) \ge f_3(\ddot{\mathbf{x}})$ with equality when $\ddot{\mathbf{x}} = \ddot{\mathbf{x}}_m$.

Proof: The proof is similar to that of Lemma III.1. ∎

Applying the lemma yields the minorized problem as

$$\underset{\ddot{\mathbf{x}}\in\mathcal{X}}{\text{maximize}}\quad \ddot{\mathbf{x}}^T(\mathbf{Q}_1+\mathbf{Q}_2)\ddot{\mathbf{x}} + \boldsymbol{\mu}^T\ddot{\mathbf{x}}, \tag{22}$$

where $\mathbf{Q}_1 = \sum_{i=j+1}^{N_r}\sum_{j=1}^{N_r}\ddot{w}_{i,j}(\mathbf{e}_i-\mathbf{e}_j)(\mathbf{e}_i-\mathbf{e}_j)^T \preceq \mathbf{0}$, $\mathbf{Q}_2 = \sum_{n=1}^{N_r}\beta_{n,1}\mathbf{e}_n\mathbf{e}_n^T \preceq \mathbf{0}$, and $\boldsymbol{\mu} = \sum_{i=j+1}^{N_r}\sum_{j=1}^{N_r}\ddot{u}_{i,j}(\mathbf{e}_i-\mathbf{e}_j) - 2\mathbf{Q}_1\ddot{\mathbf{x}}_m - 2\mathbf{Q}_2\ddot{\mathbf{x}}_m + \sum_{n=1}^{N_r}\beta_{n,2}\mathbf{e}_n$. This problem is convex and hence can be solved by existing solvers.

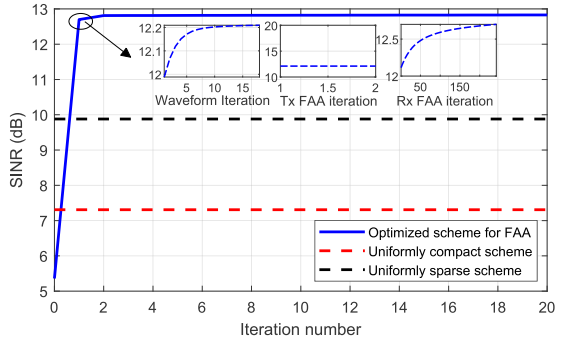

Figure 2. Comparison of different schemes for SINR improvement.

IV. Simulation Results

This section evaluates and compares the performance of the proposed FAA-MIMO radar optimization with established benchmark schemes under the following settings:

- FAA-MIMO radar: It uses $N_t = N_r = 14$ FAA elements for both transmission and reception, with a center frequency of $f_c = 3$GHz and a corresponding wavelength of $\lambda = 0.1$m. The array spans a length of $R = 2\lambda\,(N_t - 1)$ with a minimum element spacing of $r_0 = 0.5\lambda$. The waveform length is $L = 20$.
- Target and jammers: The target is located at direction 10°. Two types of jammers are considered: Full-spectrum and partial-spectrum. The full-spectrum jammers are located in the angular regions of $[5^\circ, 15^\circ]$ and $[30^\circ, 50^\circ]$ with strength of 20dB affecting the entire frequency band $[0, 1]$; the partial-spectrum jammers are located in $[-20^\circ, 0^\circ]$ with 30dB strength impacting the normalized frequency range $[0.6, 0.7]$.
- Benchmark: All schemes have the same antenna numbers. The uniformly compact scheme features a uniform array with half-wavelength spacing between elements. The uniformly sparse scheme refers to the array of the same aperture R with uniformly placed elements (i.e. spacing is 2λ).

The SINR convergence curve is presented in Fig. 2, where the waveforms are optimized in all schemes. First, we see that the proposed algorithm guarantees the monotonicity of the SINR value along the iterations and converges at 12.8 dB. Second, the enhanced SINR can be attributed to the flexible array placement enabled by the FAA scheme, and further its conjugation with the optimized waveforms. Unlike other schemes that solely optimize waveforms, the proposed approach concurrently refines the APV of the FAAs, showcasing the significance of integrating array configuration with waveform design for superior performance.

Fig. 3 presents the corresponding beampattern and energy spectral density (ESD). In principle, the joint waveform and APV design ensure much flexibility on both spatial and frequency dimensions for a better tradeoff between target illumination and jamming avoidance. Specifically, the partial-spectrum jammers are suppressed mainly in the frequency dimension by designing the waveforms. The full-spectrum jammers are eliminated in the spatial dimension. Although this type of jammers spread over multiple larger spatial regions, the combined waveform and APV design offers greater degrees of freedom for achieving precise spatial nulling. Notably, the optimized APVs, shown in Fig. 4, contribute to improved angular resolution and more effective suppression of grating lobes, surpassing conventional benchmarks with deeper nulling while not affecting the ESD.

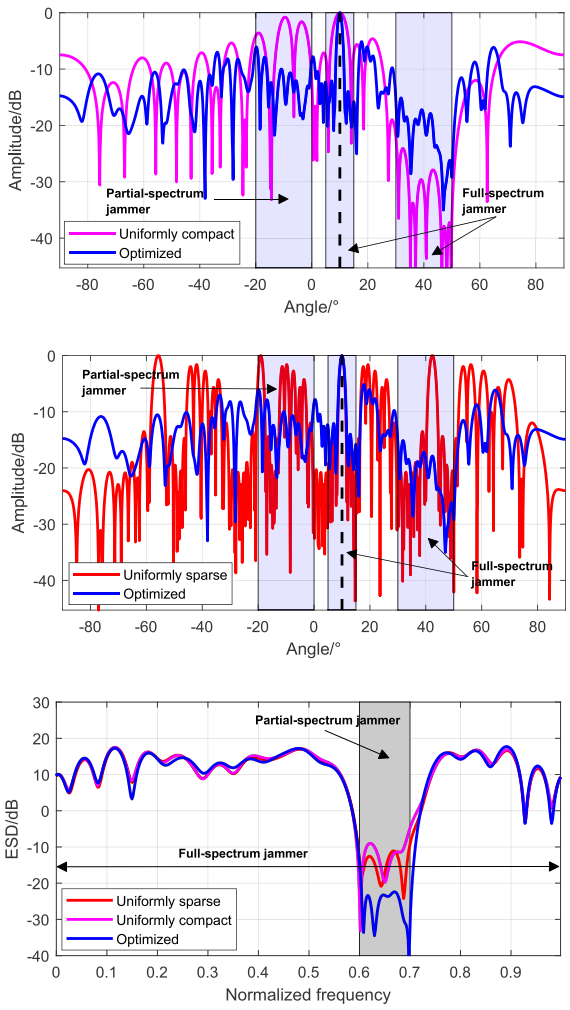

Figure 3. Beampattern and ESD. Top: Uniformly compact array versus optimized FAA; Middle: Uniformly sparse array versus optimized FAA; Bottom: Waveform ESD of all schemes.

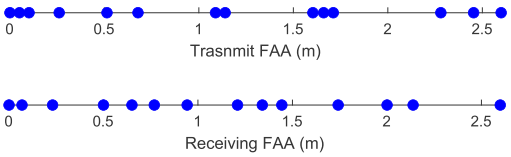

Figure 4. Designed APVs of transmit and receiving FAAs.

V. Conclusion

In this paper, the joint design of transmit waveforms and APVs in FAA-MIMO radar systems was studied to enhance target detection amidst various jamming signals. Utilizing the FAA, which allows for the dynamic positioning of array elements, provides an additional DoF for the system. For the formulated SINR maximization problem, a block majorization-minimization-based iterative algorithm was developed, with guaranteed convergence. Our findings, supported by numerical experiments, reveal that integrating APV optimization with waveform design significantly boosts SINR performance beyond what is achievable through waveform optimization alone. In particular, the dynamic FAA-based APVs offer higher flexibility, enabling superior angular resolution and multiple deep nulls simultaneously.

REFERENCES

[1] J. Li and P. Stoica, *MIMO radar signal processing*. John Wiley & Sons, 2008.

[2] G. Cui, A. De Maio, A. Farina, and J. Li, *Radar waveform design based on optimization theory*. SciTech Publishing, 2020.

[3] J. Song, P. Babu, and D. P. Palomar, "Sequence set design with good correlation properties via majorization-minimization," *IEEE Transactions on Signal Processing*, vol. 64, no. 11, pp. 2866–2879, 2016.

[4] M. Soltanalian and P. Stoica, "Computational design of sequences with good correlation properties," *IEEE Transactions on Signal Processing*, vol. 60, no. 5, pp. 2180–2193, 2012.

[5] M. Alaee-Kerahroodi, L. Wu, E. Raei, and M. R. B. Shankar, "Joint waveform and receive filter design for pulse compression in weather radar systems," *IEEE Transactions on Radar Systems*, vol. 1, pp. 212–229, 2023.

[6] A. De Maio, Y. Huang, M. Piezzo, S. Zhang, and A. Farina, "Design of optimized radar codes with a peak to average power ratio constraint," *IEEE Transactions on Signal Processing*, vol. 59, no. 6, pp. 2683–2697, 2011.

[7] L. Wu, P. Babu, and D. P. Palomar, "Transmit waveform/receive filter design for MIMO radar with multiple waveform constraints," *IEEE Transactions on Signal Processing*, vol. 66, no. 6, pp. 1526–1540, 2018.

[8] Z. Xu, Z. Xie, C. Fan, and X. Huang, "Probabilistically robust radar waveform design for extended target detection," *IEEE Transactions on Signal Processing*, vol. 70, pp. 4212–4224, 2022.

[9] A. Aubry, A. De Maio, M. Piezzo, and A. Farina, "Radar waveform design in a spectrally crowded environment via nonconvex quadratic optimization," *IEEE Transactions on Aerospace and Electronic Systems*, vol. 50, no. 2, pp. 1138–1152, 2014.

[10] L. Wu and D. P. Palomar, "Sequence design for spectral shaping via minimization of regularized spectral level ratio," *IEEE Transactions on Signal Processing*, vol. 67, no. 18, pp. 4683–4695, 2019.

[11] J. Qian, L. Venturino, M. Lops, and X. Wang, "Radar and communication spectral coexistence in range-dependent interference," *IEEE Transactions on Signal Processing*, vol. 69, pp. 5891–5906, 2021.

[12] Y. Yang and R. S. Blum, "MIMO radar waveform design based on mutual information and minimum mean-square error estimation," *IEEE Transactions on Aerospace and electronic systems*, vol. 43, no. 1, pp. 330–343, 2007.

[13] B. Tang and J. Li, "Spectrally constrained MIMO radar waveform design based on mutual information," *IEEE Transactions on Signal Processing*, vol. 67, no. 3, pp. 821–834, 2018.

[14] Z. Esmaeilbeig, A. Eamaz, K. V. Mishra, and M. Soltanalian, "Joint waveform and passive beamformer design in multi-irs-aided radar," in *ICASSP 2023 - 2023 IEEE International Conference on Acoustics, Speech and Signal Processing (ICASSP)*, 2023, pp. 1–5.

[15] Y. Huang, L. Xing, C. Song, S. Wang, and F. Elhouni, "Liquid antennas: Past, present and future," *IEEE Open Journal of Antennas and Propagation*, vol. 2, pp. 473–487, 2021.

[16] Y. Liu, Q. Wang, Y. Jia, and P. Zhu, "A frequency- and polarization-reconfigurable slot antenna using liquid metal," *IEEE Transactions on Antennas and Propagation*, vol. 68, no. 11, pp. 7630–7635, 2020.

[17] J. O. Martínez, J. R. Rodríguez, Y. Shen, K.-F. Tong, K.-K. Wong, and A. G. Armada, "Toward liquid reconfigurable antenna arrays for wireless communications," *IEEE Communications Magazine*, vol. 60, no. 12, pp. 145–151, 2022.

[18] L. Zhu, "Historical review of fluid antenna and movable antenna," *arXiv preprint arXiv:2401.02362*, 2024.

[19] K.-K. Wong, A. Shojaeifard, K.-F. Tong, and Y. Zhang, "Fluid antenna systems," *IEEE Transactions on Wireless Communications*, vol. 20, no. 3, pp. 1950–1962, 2021.

[20] K.-K. Wong and K.-F. Tong, "Fluid antenna multiple access," *IEEE Transactions on Wireless Communications*, vol. 21, no. 7, pp. 4801–4815, 2022.

[21] G. Hu, Q. Wu, K. Xu, J. Si, and N. Al-Dhahir, "Secure wireless communication via movable-antenna array," *IEEE Signal Processing Letters*, vol. 31, pp. 516–520, 2024.

[22] D. Zhang, S. Ye, M. Xiao, K. Wang, M. Di Renzo, and M. Skoglund, "Fluid antenna array enhanced over-the-air computation," *arXiv preprint arXiv:2312.15244*, 2023.

[23] L. Wu, D. P. Palomar, G. Cui, A. De Maio, A. Farina, and J. Li, "Radar waveform design via the majorization–minimization framework," in *Radar Waveform Design Based on Optimization Theory*. IET, 2020, pp. 185–220.

[24] Y. Sun, P. Babu, and D. P. Palomar, "Majorization-minimization algorithms in signal processing, communications, and machine learning," *IEEE Transactions on Signal Processing*, vol. 65, no. 3, pp. 794–816, 2017.

[25] B. Tang and J. Tang, "Joint design of transmit waveforms and receive filters for mimo radar space-time adaptive processing," *IEEE Transactions on Signal Processing*, vol. 64, no. 18, pp. 4707–4722, 2016.

[26] M. Soltanalian and P. Stoica, "Designing unimodular codes via quadratic optimization," *IEEE Transactions on Signal Processing*, vol. 62, no. 5, pp. 1221–1234, 2014.